Atmospheric Research 262 (2021) 105771

Contents lists available at ScienceDirect

Atmospheric Research

journal homepage: www.elsevier.com/locate/atmosres

Identification and spatial mapping of tracers of PM_{10} emission sources using a high spatial resolution distributed network in an urban setting

Lorenzo Massimi [a,*], Joost Wesseling [b], Sjoerd van Ratingen [b], Iqra Javed [c], Maria Agostina Frezzini [a], Maria Luisa Astolfi [d], Silvia Canepari [a], Roel Vermeulen [e]

[a] Department of Environmental Biology, Sapienza University of Rome, P. le Aldo Moro, 5, Rome 00185, Italy
[b] National Institute for Public Health and the Environment (RIVM), Antonie van Leeuwenhoeklaan 9, 3721, MA, Bilthoven, Netherlands
[c] School of Chemistry and Pharmaceutical Sciences, TUD – Technological University Dublin, City Campus, Dublin, Ireland
[d] Department of Chemistry, Sapienza University of Rome, P. le Aldo Moro, 5, Rome 00185, Italy
[e] Institute of Risk Assessment Sciences (IRAS), Utrecht University, Yalelaan 1, 3584 CL Utrecht, Netherlands.

ARTICLE INFO

Keywords:
PM_{10} composition
Chemical fractionation
Source tracer
Spatial distribution
Seasonal variation
Firework

ABSTRACT

We employed an experimental approach for high spatial resolution sampling and analysis of PM_{10}, allowing identification and spatial mapping of tracers of PM_{10} emission sources. Very-low-volume samplers were used at 17 sites in Amersfoort and at one regulatory reference site in Utrecht, The Netherlands, in a 5-month monitoring period (from September 2018 to February 2019), to assess the monthly spatial distribution of PM_{10} mass and PM_{10} chemical compounds. By performing principal component analysis on the obtained spatially-resolved data, selective and reliable source tracers were identified for soil dust (Ca^{+}, Cl^{-}, insoluble Al, Ce, Li, U and V), brake dust (insoluble Fe, Mn, Mo, Nb, Sb, Sn, W and Zr, water-soluble Fe, Mn, Mo and Sb), industrial and/or agricultural emissions (NH_4^+, water-soluble As, Co, Fe, Mn, Mo, Pb, Sb, Se, Sn and Ti), secondary organic and inorganic aerosols (water-soluble organic carbon, NO_3^- and SO_4^{2-}), biomass domestic heating (water-soluble organic carbon, levoglucosan, water-soluble Cs, Li, Rb and Tl) and New Year's Eve fireworks (K^{+}, Mg^{2+}, Na^{+}, water-soluble Al, Ba, Bi, Cr, Cu and Sr). The autumn and winter spatial mapping of the identified source tracers allowed us to effectively assess and localize the impact of the different PM_{10} sources and to evaluate the diffusion of the PM_{10} particles. This approach proved to be very effective to trace low-intensity PM_{10} sources and to map their seasonal spatial distribution. The obtained spatially-resolved chemical data can be used in further studies to evaluate spatial relationships between the concentration of PM_{10} air pollutants and adverse outcomes for human health. This approach promises to be a powerful tool for obtaining seasonal and spatially-resolved information about PM composition and sources in several study areas, having high impact on the air quality management.

1. Introduction

Over the years, various epidemiological studies have spotlighted strong correlations between the exposure to particulate matter (PM) mass concentration and the onset of asthma, lung cancer, diabetes, and cardiovascular diseases (Pope III and Dockery, 2006; Øvrevik, 2019; Schmitz et al., 2019). However, chemical characterization of PM is essential for the assessment of toxicological effects of the various PM components and for the evaluation of their impact on human health (Strak et al., 2012). Moreover, chemical analysis of PM allows identifying source tracers useful for the delineation of the impact of different emission sources.

Temporal and spatial distribution of PM compounds is highly variable, since it depends on different meteorological conditions and on the location and seasonal strength of the sources (Perrino et al., 2010; Canepari et al., 2014; Korhonen et al., 2019). However, conventional devices generally used for the collection of PM on membrane filters for subsequent analyses enable obtaining good temporal resolution, but do not allow assessing the spatial distribution of PM components with high resolution. In fact, their high cost and large size make it possible for them to be used only on a few points in large areas. The information obtained at these points is generally extended to wider areas by using mathematical models, which may not be able to correctly describe the complexity of transport and transformation processes of the PM

* Corresponding author.
E-mail address: l.massimi@uniroma1.it (L. Massimi).

https://doi.org/10.1016/j.atmosres.2021.105771
Received 25 March 2021; Received in revised form 14 July 2021; Accepted 14 July 2021
Available online 17 July 2021

compounds (Setton et al., 2010; Kloog et al., 2013; Minguillón et al., 2014).

In this study, an experimental approach for high spatial resolution sampling and analysis of PM_{10}, which allows the spatial mapping of the concentrations of PM_{10} mass and PM_{10} chemical components, was employed in the city of Amersfoort, The Netherlands. Recently developed, small-sized and very-low volume samplers (High spatial resolution sampler, HSRS; FAI Instruments, Fonte Nuova, Rome, Italy; Massimi et al., 2017; Catrambone et al., 2019) were used at 17 sites (approximately 1 km of distance between each other) in Amersfoort and at one regulatory reference site in Utrecht, during a 5-month monitoring period (from September 2018 to February 2019), to assess the monthly spatial distribution of PM_{10} compounds (water-soluble organic carbon, levoglucosan, ions, water-soluble and insoluble elements). This approach, previously described in Massimi et al. (2020b), has proven to be very effective for the impact assessment of spatially disaggregated and intensive emission sources of PM in a heavily contaminated area of Central Italy. However, it has never been used in less polluted areas with weaker emissions of PM, such as Amersfoort, The Netherlands (population ~ 156,000, non-industrialised).

This study is aimed to evaluate the efficiency of this experimental approach for the localization and impact assessment of PM_{10} sources, through the spatial mapping of chemical tracers of PM emissions, in an area with low anthropogenic impact. This approach may allow to identify local and/or temporal isolated events of air pollution, such as the burning of New Year's Eve fireworks (Greven et al., 2019). Moreover, it provides spatially-resolved chemical data on PM_{10} air pollution that can be used in further studies to relate spatial distribution of PM compounds with health effects and mortality (Knaapen et al., 2002; Toro et al., 2019; Chen and Hoek, 2020; Fischer et al., 2020).

2. Materials and methods

2.1. Study area

Amersfoort (52°9′N 5°23′E) is a medium-sized city of 63.86 km^2 located in the center of the Netherlands, in the province of Utrecht. Amersfoort has one of the largest Dutch railway junctions with its three stations (Amersfoort Centraal, Schothorst and Vathorst), it is crossed by two highways (A1 and A28), and residential biomass combustion occurs during the cold season, especially in the south of the city (Fig. 1).

In Amersfoort, throughout the year, the temperature typically ranges from 0 °C to 23 °C; the warmer season lasts about three months, from June to early September, while the colder months are December, January and February.

The average wind speed undergoes significant seasonal variations during the year. The windiest period is autumn and winter, with an average wind speed of over 18 km/h. In general, the predominant wind comes from the south-west. In the autumn-winter months, the predominant wind comes mainly from the south and sometimes from the west (Gelaro et al., 2017). Wind direction and wind speed roses for the 5-month monitoring period, compared to those of the period 2011–2020 (source of the data: https://www.knmi.nl/nederland-nu/klimatologie/uurgegevens), are reported in supplementary material S1.

2.2. Sampling sites

The sampling sites were chosen with the support of the Amersfoort city hall and the National Institute for Public Health and the Environment (RIVM, Bilthoven, Netherlands). Amersfoort city hall and RIVM recommended the best locations for the deployment of the HSRS, according to the presence of local emission sources and to their previous PM monitoring. The HSRS were installed and employed at 17 sites (MR, JA, KE, JO, CO, EL, DE, SA, OS, DI, MT, CH, ED, MA, ES, WI, MN) in

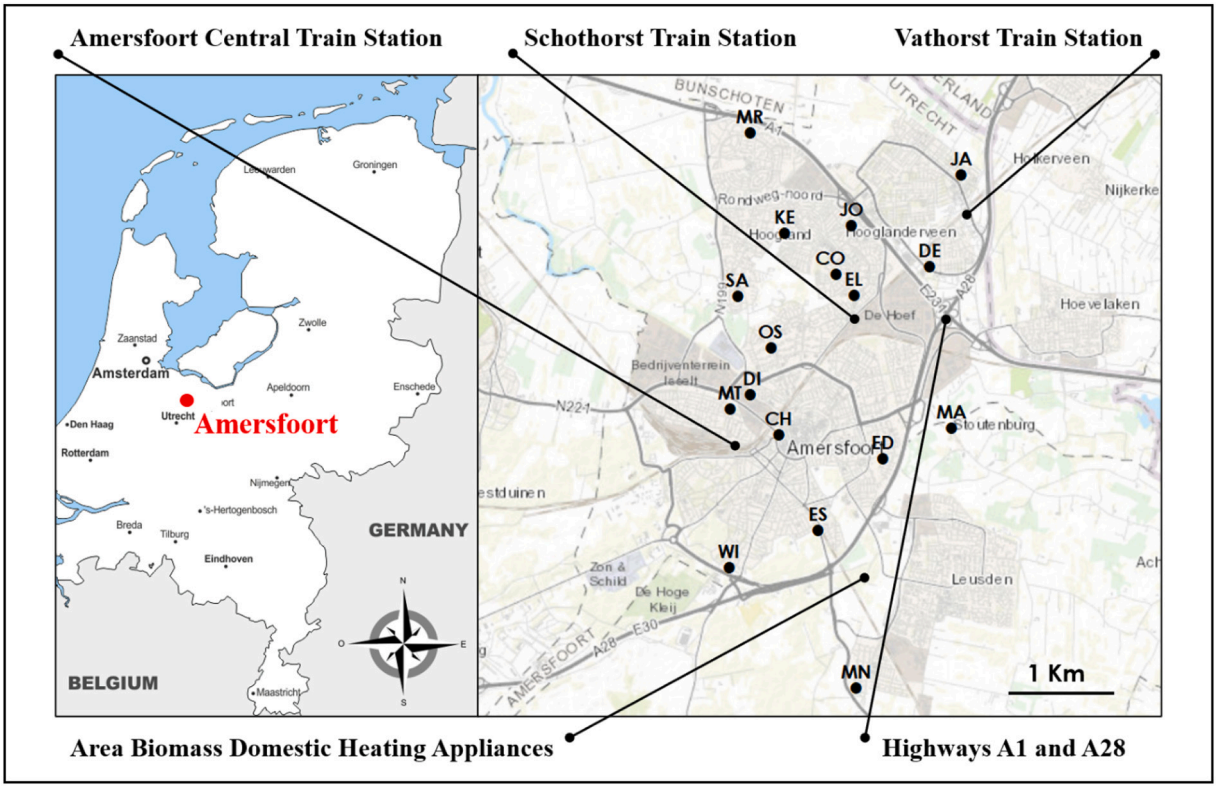

Fig. 1. Map of the 17 sampling sites in Amersfoort (Netherlands) with the location of the main local emission sources of PM (ArcMap 10.3.1, ArcGis Desktop; ESRI, Redlands, CA, USA).

Amersfoort, covering the study area with a spatial resolution of approximately 1 km (Fig. 1) and at one regulatory reference site (RS) in Utrecht, to identify reliable vehicular traffic tracers and to check PM_{10} variations not due to local emissions. At site JO, two samplers were employed to monitor sampling and analysis repeatability. All devices were installed within 6 m above ground level to ensure homogeneous sampling conditions. The geographical coordinates of the 17 sampling sites in Amersfoort and of the regulatory reference site (RS) in Utrecht are reported in Table 1. The possible local emission sources of PM in proximity of each site are detailed in Table 2, where the approximate distances (calculated using the software ArcMap 10.3.1; ArcGis Desktop; ESRI, Redlands, CA, USA) from each sampling site to potential sources are reported.

The 5-month monitoring campaign was carried out from September 8th 2018 to February 17th 2019.

2.3. Sampling equipment

The High spatial resolution sampler (HSRS; FAI Instruments, Fonte Nuova, Rome, Italy) is an automatic, small-sized and silent device (20x20x20 cm) that operates with a low flow rate: 0.5 L min^{-1}. It was equipped with 37 mm PTFE membrane filters (2 μm pore size, PALL Corporation, Port Washington, NY, USA) and worked in parallel at all sites for five 1-month sampling periods: September/October 2018, October/November 2018, November/December 2018, December/January 2019, and January/February 2019. The start and stop dates of each sampling period are reported in Table 3.

In the December/January monitoring period, one of the two samplers used at JO was stopped from 30/12/2018 to 3/1/2019 in order not to sample PM_{10} released by the burning of New Year's Eve fireworks, while the other one was left operating during the entire period.

2.4. Analytical procedure

PTFE membrane filters were weighed before and after sampling to gravimetrically determine PM_{10} mass concentrations. Each membrane filter was subjected to a chemical fractionation procedure, which consists out of extraction in water of the PM filter and in the digestion of the residue; elemental analysis was performed in both fractions (Canepari et al., 2006a, 2006b). This chemical fractionation procedure allows increasing the selectivity of the elements as source tracers (Astolfi et al., 2006; Canepari et al., 2009; Perrino et al., 2010; Astolfi et al., 2017), since, for many elements, the water-soluble and insoluble fractions are released by different PM emission sources (Massimi et al., 2020b).

Table 1
Geographical coordinates (decimal degrees) of the 17 sampling sites in Amersfoort and of the regulatory reference site (RS) in Utrecht.

Geographical coordinates of the 17 sampling sites in Amersfoort		
	Latitude	Longitude
MR	52.204549°	5.376669°
JA	52.197903°	5.431991°
KE	52.188428°	5.385851°
JO	52.189775°	5.403229°
CO	52.181914°	5.399245°
EL	52.178557°	5.404134°
DE	52.18313°	5.423743°
SA	52.178312°	5.37347°
OS	52.170157°	5.382377°
DI	52.162568°	5.376833°
MT	52.160291°	5.371474°
CH	52.156056°	5.384303°
ED	52.152208°	5.411654°
MA	52.157256°	5.42963°
ES	52.140702°	5.394428°
WI	52.134736°	5.371209°
MN	52.115462°	5.404635°
Geographical coordinates of the regulatory reference site in Utrecht		
	Latitude	Longitude
RS	52.105862°	5.124655°

In short, the polymethylpentene support ring was removed from each PM filter, which underwent ultrasound assisted extraction for 30 min in 10 mL of deionized water (Arioso UP 900 Integrate Water Purification System, Cole-Parmer Co Ltd., Saint Neots, England, UK). The water-extracted solution was then filtered through a cellulose nitrate filter (pore size 0.45 μm, Merck Millipore Ltd., Billerica, MA, USA). The PM filter containing the insoluble residue and the cellulose nitrate filter used for the filtration were then subjected to a microwave assisted acid digestion (Ethos Touch Control with Q20 rotor, Milestone, Bergamo, Italy) using 2 mL of ultrapure HNO_3 (67%; Promochem, LGC Standards GmbH, Wesel, Germany) and 1 mL of H_2O_2 (30%; Promochem, LGC Standards GmbH, Wesel, Germany). The digested solution was then diluted to 50 mL with deionized water and filtered using syringe filters (cellulose nitrate; diameter 25 mm, pore size 0.45 μm, GVS Filter Technology, Morecambe, England, UK).

Elements in the water-soluble (Al_s, As_s, Ba_s, Bi_s, Co_s, Cr_s, Cs_s, Cu_s, Fe_s, Li_s, Mn_s, Mo_s, Pb_s, Rb_s, Sb_s, Se_s, Sn_s, Sr_s, Ti_s, Tl_s) and insoluble (Al_i, Ce_i, Fe_i, Li_i, Mn_i, Mo_i, Nb_i, Sb_i, Sn_i, U_i, V_i, W_i, Zr_i) fractions were analyzed by a quadrupole inductively coupled plasma mass spectrometer (ICP-MS; model 820-MS; Bruker, Bremen, Germany) equipped with a glass nebulizer (0.4 mL min^{-1}; Analytik Jena AG, Jena, Germany). For each element, the external standard calibration curve was performed in the range 1–500 μg L^{-1} by serially diluting stock standard solutions (1000 ± 2 mg L^{-1}; Exaxol Italia Chemical Manufacturers Srl, Genoa, Italy; Ultra Scientific, North Kingstown, RI, USA; Merck Millipore Ltd., Billerica, MA, USA). To control nebulizer efficiency, Y (1000 ± 2 mg L^{-1}; Panreac Química, Barcelona, Spain) was set at 5 μg L^{-1} as internal standard for all measurements. The instrumental conditions and performance of the method are detailed in Astolfi et al. (2020) and Canepari et al. (2009) respectively.

In addition to the elements, the soluble fraction of PM was analyzed for water-soluble organic carbon (WSOC), ions and levoglucosan (LVG).

WSOC was analyzed by TOC-VCSH (Shimadzu Corporation, Kyoto, Japan), using the NPOC (non-purgeable organic carbon) procedure (Saarikoski et al., 2007). An aliquot of 0.5 mL of the water-extracted solution of PM, diluted 1:10 with deionized water and 100 μL of HCl 10 M (Promochem, LGC Standards GmbH, Wesel, Germany) was used for the WSOC analysis.

Ions (Ca^{2+}, Cl^-, K^+, Mg^{2+}, Na^+, NH_4^+, NO_3^-, SO_4^{2-}) were analyzed by ion chromatography (IC) (ICS1000, Dionex Co., CA, USA) using a total of 1 mL of the water-extracted solution.

Finally, an aliquot of 0.5 mL of the extracted solution, diluted 1:2 with deionized water, was analyzed for LVG by High-Performance Anion-Exchange Chromatography with Pulsed Amperometric Detection (HPAEC-PAD). A Dionex DX-500 series ion chromatograph equipped with a DC ICS-3000 oven, a GP40 Gradient Pump, and a CarboPac™ PA10 analytical and guard column was used for LVG analysis; a Dionex ED50/ED50A Electrochemical Cell equipped with disposable gold electrodes was employed as electrochemical detector (Perrino et al., 2019).

2.5. Data analysis

The detection limit (LOD) of each analyte was set at 3 times the standard deviation (SD) of 10 replicate blank determinations.

Duplicate concentration data obtained for each monitoring period (except for December/January period) at site JO for PM_{10} and for the analyzed PM_{10} compounds were used to calculate the relative standard deviations (RSDs) in order to assess the sampling and analysis repeatability. The RSDs obtained in the December/January monitoring period are not indicative of the sampling and analysis repeatability, since one of the two samplers used at JO was stopped from 30/12/2018 to 3/1/2019 to assess the release of PM_{10} chemical components due to the burning of

Table 2
Approximate distances (m) from each of the 17 sampling site in Amersfoort to potential local emission sources of PM; the shorter distances of the sources from each site are indicated in bold.

Sapling Site	Closest Commercial Area	Closest Trafficked Street	Highway A1	Highway A28	Closest Bus Stop	Closest Traffic Light (T) and/or Roundabout (R)	Closest Railway Track	Closest Train Station	Closest Farmland	Landfill
JA	2000	**110**	1800	**500**	220	250 (R)	520	**600**	400	2200
MR	1200	800	**200**	4900	**70**	830 (T)	3600	3800	**300**	**1000**
JO	400	150	**280**	2400	200	190 (T)	1200	1700	1700	**1300**
KE	800	300	1300	3200	240	720 (T) 560 (R)	1900	2000	1400	**1600**
CO	400	600	1000	2000	280	700 (T)	800	850	2400	2100
DE	**150**	**25**	**340**	750	180	560 (T) **70 (R)**	**260**	1200	900	2700
EL	350	270	1000	1700	**90**	330 (T)	290	**400**	2300	2500
SA	1200	270	2700	3600	190	440 (T) 380 (R)	1900	2100	350	3000
OS	700	240	2800	2700	100	470 (T) 220 (R)	870	1500	600	3600
MA	400	600	1500	750	500	800 (T)	1300	2300	**0**	5300
ED	500	770	2700	**280**	220	250 (T)	1600	2600	400	5500
DI	**0**	220	3600	3000	160	350 (T) 500 (R)	620	1000	1300	4600
MT	**270**	170	4100	3100	150	260 (T)	700	**700**	1500	4800
CH	450	140	3800	2200	**40**	**50 (T)**	**200**	800	2200	5000
ES	1300	**30**	4500	650	160	**100 (T)**	**60**	2000	700	6700
WI	2800	170	6000	**500**	200	280 (T)	1800	2100	2300	7600
MN	900	140	6500	2100	220	170 (T)	800	1000	**240**	9600

Table 3
Start and stop dates of the five sampling periods.

Start and stop dates of the five sampling periods				
Season	Sampling	Period	Start date	Stop date
Autumn	1°	September/October	8/9/2019	7/10/2018
	2°	October/November	13/10/2018	11/11/2018
	3°	November/December	17/11/2018	12/12/2018
Winter	4°	December/January	18/12/2018	13/1/2019
	5°	January/February	19/1/2019	17/2/2019

New Year's Eve fireworks. In the December/January period the chemical compounds with RSDs >50% were considered to be related to PM_{10} by the use of fireworks. LODs and RDSs of all the analyzed variables are reported in supplementary material S1.

Concentration data determined at each site in the September/October, October/November and November/December monitoring periods were averaged to obtain autumn mean concentrations, while data obtained for December/January and January/February periods were averaged to obtain winter mean concentrations.

2.6. Principal component analysis

Emission tracers of the main PM_{10} sources were identified and clustered by performing principal component analysis (PCA) on the concentration data of PM_{10} and of all the analyzed PM_{10} components.

The matrix of the data (3960 data points) used for the PCA is composed of 90 samples: 18 samples (one sample per site) for each of the 5 sampling periods, and of 44 variables: PM_{10} mass and WSOC, LVG, Ca^{2+}, Cl^{-}, K^{+}, Mg^{2+}, Na^{+}, NH_4^{+}, NO_3^{-}, SO_4^{2-}, Al_s, As_s, Ba_s, Bi_s, Co_s, Cr_s, Cs_s, Cu_s, Fe_s, Li_s, Mn_s, Mo_s, Pb_s, Rb_s, Sb_s, Se_s, Sn_s, Sr_s, Ti_s, Tl_s, Al_i, Ce_i, Fe_i, Li_i, Mn_i, Mo_i, Nb_i, Sb_i, Sn_i, U_i, V_i, W_i and Zr_i concentration (ng m^{-3}). The matrix of the data was transformed by column mean centering and row and column autoscaling before performing the PCA (Conti et al., 2007; Massimi et al., 2017). PCA was carried out using the statistical software CAT (Chemometric Agile Tool; Leardi et al., n.d) based on the R-project for statistical computing, Ver. 3.0, 32-bit.

2.7. Data interpolation and spatial mapping

Spatially-resolved data of the autumn and winter monitoring periods were interpolated by using the ordinary kriging (OK) method (Johnston et al., 2001) to create a continuous surface from the 17 measured sample points in Amersfoort and predict the values at unmeasured points (Kumar et al., 2007). Ordinary kriging is a geostatistical interpolation method in which the distance and the degree of variation between known data points are considered to estimate values in unknown locations by using as estimator a linear combination of the observed values with weights, which are derived from a semivariogram function (Xie et al., 2011; Paramasivam and Venkatramanan, 2019). The spherical semivariogram model was used to interpolate the high spatial resolution data and the experimental semivariances were fitted by weighted least-squares approximation (Jian et al., 1996).

The autumn and winter spatial distribution of PM_{10} and PM_{10} chemical components was mapped using the software ArcMap 10.3.1 (ArcGis Desktop; ESRI, Redlands, CA, USA).

3. Results and discussion

3.1. Concentrations of PM_{10} mass and PM_{10} chemical compounds

From Fig. 2, we can observe an increase in PM_{10} mass concentration at all the sampling sites in winter, especially in the January/February monitoring period. This increase can be explained by the greater intensity of typical winter sources such as biomass domestic heating and by a less efficient mixing of the lower atmosphere in the colder period, which leads to frequent temperature inversions and to stronger atmospheric stability (Hendriks et al., 2013).

Mean PM_{10} mass concentration at all the sites was very low: 17 μg m^{-3} in autumn and 22 μg m^{-3} in winter. As it can be seen from Tables 4 and 5, in which autumn and winter concentrations of PM_{10} mass and PM_{10} components are reported, the highest PM_{10} mass concentration (34 μg m^{-3}) was found in winter at ED, which is the closest site to the highway A28 (Table 2), located in an area where biomass domestic heating appliances were used (Fig. 1). Relatively high winter PM_{10} mass concentration was recorded also at CO (30 μg m^{-3}) and at MN (29 μg m^{-3}), which are sites located, respectively, near the highway A1 and in the area where domestic biomass combustion occurred in the colder

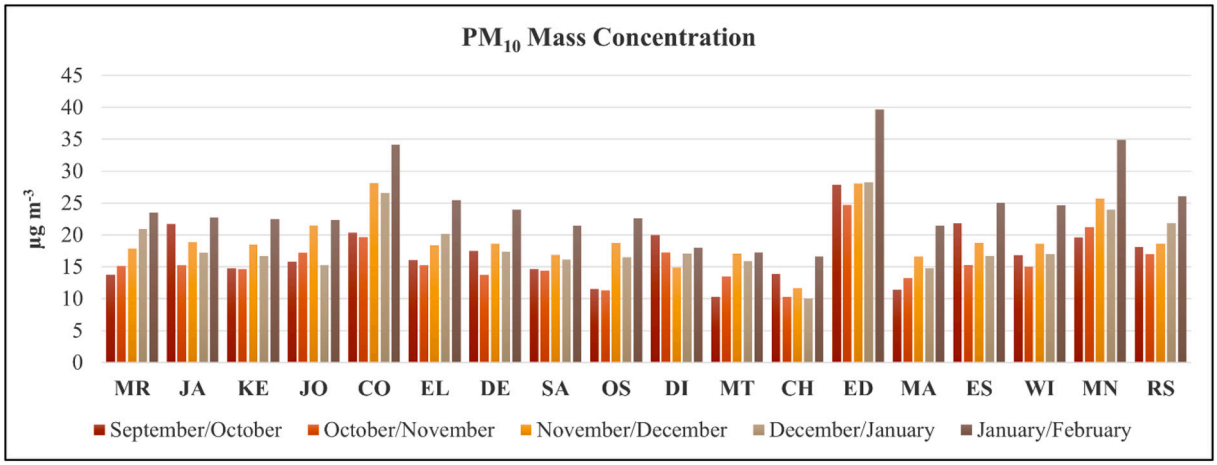

Fig. 2. PM_{10} mass concentrations (μg m^{-3}) obtained at the 17 sampling sites in Amersfoort and at the regulatory reference site (RS) in Utrecht in the 5-month monitoring period.

period. The lowest PM_{10} mass concentration was found in autumn at CH (12 μg m^{-3}), located in the city center, while the highest autumn PM_{10} mass concentrations were recorded at ED, CO and MN (27, 23 and 22 μg m^{-3}, respectively).

From Tables 4 and 5, we can observe that the concentrations of WSOC, LVG, K^+, Mg^{2+}, Na^+, NH_4^+, NO_3^-, SO_4^{2-} and of all the elements in the water-soluble fraction of PM_{10} were higher in winter, while the concentrations of Ca^+, Cl^- and insoluble elements were higher in autumn. This different behavior can be reasonably explained by the different emission sources that release these PM_{10} components. In fact, WSOC, LVG, K^+, Mg^{2+}, Na^+, NH_4^+, NO_3^-, SO_4^{2-} and water-soluble elements are generally in the fine fraction of PM (Canepari et al., 2019), originated by the accumulation of ultrafine particles released by combustion sources, such as biomass domestic heating, which is a winter emission source, and the burning of New Year's Eve fireworks. On the contrary, Ca^+, Cl^- and insoluble elements are usually in the coarse fraction of PM, associated to soil (Ca^+, Cl^-, Al_i, Ce_i, Li_i, U_i and V_i; Canepari et al., 2008; Pant and Harrison, 2013) or brake abrasion dust (Fe_i, Mn_i, Mo_i, Nb_i, Sb_i, Sn_i, W_i and Zr_i; Querol et al., 2012; Namgung et al., 2016), whose resuspension is greater in autumn (Massimi et al., 2020b). Concentrations of PM_{10} mass and PM_{10} chemical compounds obtained at all sampling sites in each monitoring period are reported in supplementary material S2.

3.2. *Identification of PM_{10} source tracers*

To identify emission tracers of the main PM_{10} sources acting in Amersfoort during the 5-month monitoring period and to cluster the samples depending on their spatial and temporal distribution, explorative PCA was performed.

Three significant components accounting for 73.3% of the total variance were obtained (the scores and loadings are shown in supplementary material S3); the variance explained by each component is: 32.9%, 22.9% and 17.5%. First component (PC1) clusters the samples (scores) depending on the monthly concentration variability of PM_{10} chemical compounds (loadings). Therefore, samples collected in autumn (in the September/October, October/November and November/December monitoring periods), in which higher concentrations of Ca^+, Cl^- and insoluble elements were obtained (Tables 4 and 5), are almost all plotted on the left part of the score plot. On the contrary, winter samples (of the December/January and January/February periods), containing higher concentrations of WSOC, LVG, K^+, Mg^{2+}, Na^+, NH_4^+, NO_3^-, SO_4^{2-} and water-soluble elements, are mostly plotted on the right part of the score plot.

From Fig. 3, we can observe that for each monitoring period, samples collected at DI, MT, CH and MA, where higher concentrations of crustal components of PM_{10} (Ca^+, Cl^-, Al_i, Ce_i, Li_i, U_i and V_i) were found, are separated along PC1 from samples collected at CO, ED and MN, containing higher concentrations of WSOC, LVG, NH_4^+, NO_3^-, SO_4^{2-} and water-soluble elements (Tables 4 and 5). Indeed, Ca^+, Cl^-, Al_i, Ce_i, Li_i, U_i and V_i are all clustered as soil dust tracers in the group A of the loading plot (panel b), while WSOC, LVG, NH_4^+, NO_3^-, SO_4^{2-}, As_s, Co_s, Cs_s, Fe_s, Li_s, Mn_s, Mo_s, Pb_s, Rb_s, Sb_s, Se_s, Sn_s, Ti_s and Tl_s are clustered in the groups C, D and E.

Group C contains the water-soluble fraction of elements (Fe_s, Mn_s, Mo_s and Sb_s) presumably released by industrial emissions (Kim and Jo, 2006; Mooibroek et al., 2011; Mbengue et al., 2014) and partly emitted by brake abrasion (Garg et al., 2000; Thorpe and Harrison, 2008), along with their insoluble fraction (group B), which is more strongly associated to brake dust (Abbasi et al., 2012; Kam et al., 2013; Massimi et al., 2020b).

On the other hand, group D is composed of water-soluble elements (As_s, Co_s, Pb_s, Se_s, Sn_s and Ti_s) and NH_4^+, whose release can be more reliably attributed to industrial (Belis et al., 2015; Mooibroek et al., 2011; Fernández-Camacho et al., 2012; Park et al., 2014) and/or agricultural sources (Battye et al., 2003; Shen et al., 2011). In fact, NH_4^+ is formed in the atmosphere by the protonation of NH_3, which is mainly released by the decomposition of organic matter from animal farming and by the use of nitrogen fertilizers in agriculture (Pozzer et al., 2017).

Finally, group E contains secondary inorganic ions (NO_3^-, SO_4^{2-}) and biomass burning tracers (WSOC, LVG, Cs_s, Li_s, Rb_s and Tl_s), which were most likely emitted by biomass domestic heating sources (Cheng et al., 2014; Frasca et al., 2018; Simonetti et al., 2018; Massimi et al., 2020a), especially in winter at CO, ED and MN (Tables 4 and 5). In fact, LVG is a highly selective biomass burning tracer (Simoneit et al., 2004; Engling et al., 2006; Sullivan et al., 2008), since it is a dominant organic component emitted in fine wood smoke (Simoneit et al., 1999; Schauer et al., 2001). Water-soluble Cs, Li, Rb and Tl are also known to be produced by wood burning and they can be used as effective biomass domestic heating tracers (Canepari et al., 2014; Frasca et al., 2018; Massimi et al., 2020b). Water-soluble organic carbon is a less selective tracer, since it is also derived from biogenic materials, soil dust and fuel combustion (Urban et al., 2012); despite this, a considerable fraction of WSOC is generally produced by the combustion of biomass for residential heating (Graham et al., 2002; Massimi et al., 2020a). Moreover, WSOC is an indicator of water-soluble secondary organic particles (Weber et al., 2007; Ervens et al., 2011) that can be formed during the aging process of biomass burning smoke (Lee et al., 2008; Adler et al., 2011). On the other hand, NO_3^- and SO_4^{2-}, which are clustered in the same group, are tracers of secondary inorganic aerosols (secondary

Table 4
Concentrations of PM_{10} mass (μg m^{-3}) and PM_{10} chemical compounds (ng m^{-3}) obtained at the 17 sampling sites in Amersfoort and at the regulatory reference site (RS) in Utrecht in the autumn monitoring period.

	MR	JA	KE	JO	CO	EL	DE	SA	OS	DI	MT	CH	ED	MA	ES	WI	MN	RS
PM_{10}	16	19	16	18	23	17	17	15	14	17	14	12	27	14	19	17	22	18
WSOC	3243	4185	4260	3615	5955	3675	2340	2370	2870	2910	2820	1531	6256	2804	2831	3270	6015	4175
LVG	644	639	698	678	1119	618	658	518	565	556	771	546	829	583	599	851	919	613
Ca^{2+}	207	360	217	308	324	226	256	230	333	344	257	210	388	242	307	204	294	281
Cl^-	3056	2506	2307	3084	4220	2677	2722	2408	2200	2414	2241	1266	3413	2086	2573	2048	3624	3385
K^+	105	114	118	148	155	106	206	114	156	147	119	71	244	164	180	95	215	200
Mg^{2+}	66	67	66	79	101	69	70	63	60	75	52	39	95	58	62	53	88	78
Na^+	520	493	580	768	767	502	602	463	434	666	413	366	817	482	579	400	699	591
NH_4^+	794	709	683	938	1280	738	774	707	610	451	667	358	1062	576	723	631	1117	771
NO_3^-	1338	1244	1285	1647	2041	1337	1299	1185	1320	991	1144	602	1751	1032	1215	1093	1804	1437
SO_4^{2-}	553	491	566	714	857	557	552	497	496	377	470	316	763	439	506	482	792	607
Al_s	4.2	5.7	7.0	9.6	13	6.5	7.9	8.2	13	8.0	5.6	4.4	9.4	5.6	6.5	8.1	13	5.8
As_s	0.41	0.43	0.53	0.50	0.84	0.49	0.37	0.42	0.42	0.38	0.45	0.30	0.71	0.36	0.37	0.46	0.62	0.35
Ba_s	2.9	3.2	2.9	3.4	3.5	4.4	3.9	3.8	2.6	2.3	2.9	1.7	3.8	1.8	2.7	2.8	3.4	6.7
Bi_s	0.019	0.019	0.022	0.027	0.034	0.021	0.025	0.025	0.019	0.013	0.019	0.014	0.034	0.020	0.021	0.022	0.033	0.019
Co_s	0.024	0.033	0.033	0.034	0.049	0.034	0.032	0.032	0.037	0.032	0.028	0.019	0.058	0.026	0.047	0.039	0.045	0.037
Cr_s	0.17	0.22	0.20	0.23	0.31	0.21	0.19	0.18	0.21	0.19	0.20	0.14	0.30	0.17	0.20	0.21	0.28	0.22
Cs_s	0.018	0.020	0.022	0.023	0.031	0.021	0.019	0.018	0.019	0.019	0.018	0.012	0.030	0.018	0.017	0.020	0.031	0.022
Cu_s	4.2	4.8	4.0	5.8	7.3	6.1	6.8	4.3	3.9	7.5	3.8	2.5	6.9	3.4	5.8	5.1	5.2	13
Fe_s	10	15	14	16	22	13	14	11	13	12	14	6.4	24	11	16	14	21	17
Li_s	0.028	0.051	0.047	0.049	0.069	0.043	0.040	0.040	0.042	0.050	0.041	0.023	0.073	0.037	0.039	0.044	0.070	0.053
Mn_s	2.4	2.7	2.6	2.9	3.9	2.8	2.8	2.5	2.4	2.7	2.3	1.4	4.0	2.2	2.6	2.7	3.6	3.5
Mo_s	0.29	0.34	0.30	0.36	0.50	0.40	0.32	0.30	0.32	0.38	0.33	0.23	0.43	0.26	0.30	0.32	0.42	0.37
Pb_s	0.91	1.1	1.3	1.4	2.0	1.1	1.1	1.2	1.2	0.8	1.1	0.57	2.0	1.1	1.0	1.4	2.0	0.8
Rb_s	0.21	0.23	0.27	0.27	0.36	0.29	0.26	0.22	0.25	0.35	0.22	0.16	0.38	0.24	0.27	0.29	0.37	0.22
Sb_s	0.41	0.47	0.45	0.54	0.67	0.51	0.55	0.41	0.41	0.44	0.39	0.27	0.75	0.39	0.47	0.49	0.63	0.66
Se_s	0.31	0.32	0.38	0.41	0.51	0.47	0.31	0.39	0.34	0.38	0.32	0.27	0.51	0.35	0.33	0.38	0.59	0.42
Sn_s	0.14	0.16	0.15	0.19	0.23	0.16	0.16	0.14	0.15	0.11	0.13	0.076	0.23	0.13	0.16	0.16	0.21	0.18
Sr_s	1.1	1.5	1.2	1.3	1.6	1.3	1.2	1.3	1.1	1.5	1.0	0.7	1.6	1.0	1.1	1.1	1.7	1.4
Ti_s	0.078	0.090	0.090	0.12	0.17	0.10	0.090	0.082	0.11	0.076	0.10	0.053	0.18	0.081	0.11	0.093	0.15	0.11
Tl_s	0.019	0.022	0.023	0.025	0.034	0.023	0.021	0.020	0.020	0.019	0.019	0.015	0.035	0.019	0.020	0.024	0.034	0.023
Al_i	69	151	134	126	87	128	164	86	124	153	123	67	129	64	54	104	104	76
Ce_i	0.19	0.18	0.14	0.16	0.20	0.13	0.18	0.13	0.16	0.19	0.11	0.10	0.19	0.11	0.14	0.14	0.19	0.17
Fe_i	242	270	214	301	266	250	394	226	219	323	192	154	350	165	306	232	285	649
Li_i	0.061	0.056	0.054	0.054	0.068	0.053	0.072	0.054	0.065	0.075	0.059	0.033	0.078	0.050	0.051	0.061	0.066	0.048
Mn_i	3.0	4.0	3.2	3.7	3.7	3.2	4.3	3.0	3.0	4.2	2.9	2.4	4.4	2.4	3.3	3.0	3.8	5.6
Mo_i	0.27	0.36	0.28	0.37	0.37	0.33	0.45	0.25	0.31	0.49	0.28	0.22	0.48	0.20	0.39	0.31	0.40	0.71
Nb_i	0.028	0.031	0.027	0.035	0.035	0.028	0.040	0.030	0.028	0.045	0.024	0.023	0.048	0.021	0.033	0.033	0.032	0.080
Sb_i	0.81	1.2	0.85	1.0	1.1	0.65	1.2	0.90	0.85	1.1	0.78	0.87	1.5	0.79	0.88	1.1	1.0	1.8
Sn_i	1.7	2.1	1.9	2.5	2.5	1.8	2.9	1.9	1.7	2.5	1.4	1.4	3.2	1.5	2.4	2.3	2.4	5.1
U_i	0.0030	0.0045	0.0034	0.0036	0.0054	0.0034	0.0048	0.0035	0.0048	0.0047	0.0040	0.0027	0.0045	0.0038	0.0039	0.0035	0.0048	0.0046
V_i	0.22	0.16	0.22	0.22	0.28	0.18	0.25	0.16	0.14	0.30	0.17	0.15	0.25	0.18	0.25	0.19	0.34	0.28
W_i	0.022	0.043	0.042	0.037	0.068	0.030	0.034	0.037	0.036	0.055	0.035	0.029	0.062	0.029	0.058	0.046	0.056	0.041
Zr_i	0.45	0.50	0.36	0.54	0.50	0.44	0.76	0.44	0.40	0.63	0.36	0.30	0.64	0.28	0.53	0.42	0.48	1.2

Table 5
Concentrations of PM_{10} mass (μg m^{-3}) and PM_{10} chemical compounds (ng m^{-3}) obtained at the 17 sampling sites in Amersfoort and at the regulatory reference site (RS) in Utrecht in the winter monitoring period.

	MR	JA	KE	JO	CO	EL	DE	SA	OS	DI	MT	CH	ED	MA	ES	WI	MN	RS
PM_{10}	22	20	20	19	30	23	21	19	20	18	17	13	34	18	21	21	29	24
WSOC	5011	4755	5175	5430	6510	5525	5070	4875	5220	1977	4057	2422	6960	3990	5550	4170	6780	5040
LVG	1772	1212	1270	1803	2451	1590	1165	1374	1657	763	1383	863	2764	1424	1465	1404	2291	1344
Ca^{2+}	127	99	126	95	133	176	154	103	203	180	133	77	141	106	94	82	257	173
Cl^{-}	1376	1239	1224	688	1609	1725	1141	1072	1120	1375	1447	680	1821	996	1101	966	1659	1577
K^{+}	648	384	364	279	519	430	265	342	488	304	297	159	460	209	222	230	374	380
Mg^{2+}	142	117	104	71	143	118	104	102	129	89	96	62	160	90	93	92	143	140
Na^{+}	821	715	784	532	956	947	709	675	1076	695	662	452	1083	635	677	657	1078	980
NH_4^{+}	1346	1093	1186	1363	1395	1453	1244	1161	1172	592	836	669	1786	1120	1398	1107	1350	1424
NO_3^{-}	3763	3482	3406	3867	5637	4278	3500	3168	3391	2337	2272	2005	5751	3240	3832	3235	5708	4054
SO_4^{2-}	1528	1292	1256	1212	1981	1754	1158	1243	1204	701	939	762	1927	1075	1309	1089	1837	1445
Al_s	22	19	13	19	23	15	16	14	17	13	11	9.6	22	8.4	14	11	18	16
As_s	0.39	0.34	0.62	0.51	0.65	0.50	0.31	0.43	0.51	0.26	0.47	0.30	0.91	0.42	0.33	0.32	0.70	0.34
Ba_s	35	25	15	14	22	14	15	19	30	20	15	7.6	25	11	13	13	19	22
Bi_s	0.48	0.62	0.34	0.37	0.61	0.33	0.35	0.34	0.37	0.35	0.31	0.13	0.59	0.24	0.28	0.26	0.45	0.40
Co_s	0.029	0.039	0.033	0.030	0.041	0.034	0.029	0.034	0.023	0.024	0.025	0.020	0.060	0.026	0.055	0.034	0.050	0.037
Cr_s	0.67	0.54	0.43	0.47	0.77	0.47	0.43	0.44	0.44	0.41	0.41	0.29	0.78	0.35	0.43	0.41	0.62	0.54
Cs_s	0.028	0.026	0.029	0.033	0.040	0.030	0.028	0.026	0.029	0.013	0.026	0.020	0.047	0.025	0.030	0.026	0.042	0.029
Cu_s	18	14	9.1	8.4	16	12	13	10	8.7	13	8.7	5.5	17	6.8	10	8.3	14	20
Fe_s	14	17	20	16	31	21	18	17	13	11	12	12	37	14	24	20	27	21
Li_s	0.059	0.066	0.054	0.041	0.080	0.064	0.061	0.054	0.058	0.046	0.053	0.033	0.096	0.048	0.058	0.051	0.084	0.064
Mn_s	2.8	2.7	2.8	2.4	4.0	3.2	2.8	2.6	2.4	2.1	2.1	1.7	4.4	2.3	3.0	2.4	3.7	3.7
Mo_s	0.32	0.33	0.33	0.38	0.50	0.41	0.33	0.26	0.33	0.28	0.30	0.25	0.51	0.29	0.37	0.30	0.51	0.37
Pb_s	1.4	1.4	1.7	1.8	2.5	1.7	1.3	1.3	1.6	1.1	1.2	1.2	3.8	1.4	1.7	1.5	2.5	1.1
Rb_s	0.43	0.37	0.36	0.40	0.51	0.38	0.35	0.31	0.32	0.31	0.33	0.30	0.56	0.38	0.29	0.26	0.41	0.32
Sb_s	0.48	0.46	0.52	0.54	0.72	0.58	0.50	0.45	0.45	0.37	0.40	0.34	0.86	0.46	0.62	0.48	0.74	0.67
Se_s	0.50	0.43	0.45	0.57	0.75	0.54	0.41	0.36	0.44	0.31	0.38	0.32	0.74	0.39	0.54	0.43	0.70	0.46
Sn_s	0.21	0.20	0.24	0.29	0.32	0.24	0.21	0.19	0.23	0.15	0.16	0.11	0.31	0.20	0.33	0.22	0.42	0.24
Sr_s	14	8.4	4.7	4.5	8.9	5.6	6.7	5.3	11	9.1	5.4	2.6	9.3	4.1	4.1	4.3	6.8	8.3
Ti_s	0.16	0.14	0.15	0.17	0.27	0.17	0.14	0.17	0.14	0.11	0.11	0.089	0.25	0.13	0.17	0.14	0.26	0.18
Tl_s	0.025	0.023	0.029	0.033	0.038	0.030	0.024	0.022	0.024	0.015	0.023	0.018	0.044	0.023	0.026	0.023	0.037	0.026
Al_i	115	120	132	58	63	79	93	102	108	95	81	31	72	105	32	83	71	119
Ce_i	0.29	0.18	0.12	0.10	0.16	0.15	0.16	0.17	0.13	0.17	0.13	0.093	0.19	0.10	0.13	0.16	0.16	0.21
Fe_i	248	178	180	150	253	267	324	210	187	211	153	132	250	174	224	246	217	508
Li_i	0.052	0.041	0.034	0.026	0.044	0.047	0.059	0.022	0.022	0.035	0.027	0.019	0.028	0.021	0.020	0.038	0.049	0.045
Mn_i	3.3	2.7	2.8	2.2	3.2	3.2	3.5	2.7	2.5	3.2	2.3	1.9	3.1	2.4	2.5	3.2	2.8	4.8
Mo_i	0.28	0.29	0.26	0.19	0.37	0.37	0.45	0.27	0.23	0.30	0.22	0.20	0.39	0.25	0.31	0.33	0.26	0.59
Nb_i	0.033	0.031	0.023	0.019	0.029	0.034	0.050	0.025	0.020	0.026	0.021	0.024	0.047	0.029	0.037	0.032	0.029	0.081
Sb_i	0.95	0.85	0.76	0.63	1.0	1.0	1.3	0.64	0.77	0.73	0.64	0.85	1.4	1.0	0.94	1.0	0.97	1.8
Sn_i	2.4	2.1	2.0	1.9	2.8	2.6	3.2	2.0	1.7	1.9	1.6	1.5	3.0	1.9	2.5	2.5	2.6	4.6
U_i	0.0025	0.0047	0.0039	0.0017	0.0033	0.0033	0.0040	0.0051	0.0036	0.0030	0.0025	0.0026	0.0030	0.0033	0.0022	0.0046	0.0036	0.0045
V_i	0.31	0.11	0.22	0.16	0.23	0.23	0.31	0.17	0.11	0.21	0.22	0.20	0.23	0.11	0.20	0.20	0.22	0.51
W_i	0.038	0.034	0.037	0.025	0.044	0.041	0.047	0.025	0.028	0.042	0.027	0.026	0.053	0.035	0.059	0.041	0.036	0.041
Zr_i	0.43	0.36	0.32	0.27	0.44	0.48	0.62	0.40	0.28	0.43	0.30	0.28	0.43	0.32	0.39	0.40	0.35	0.84

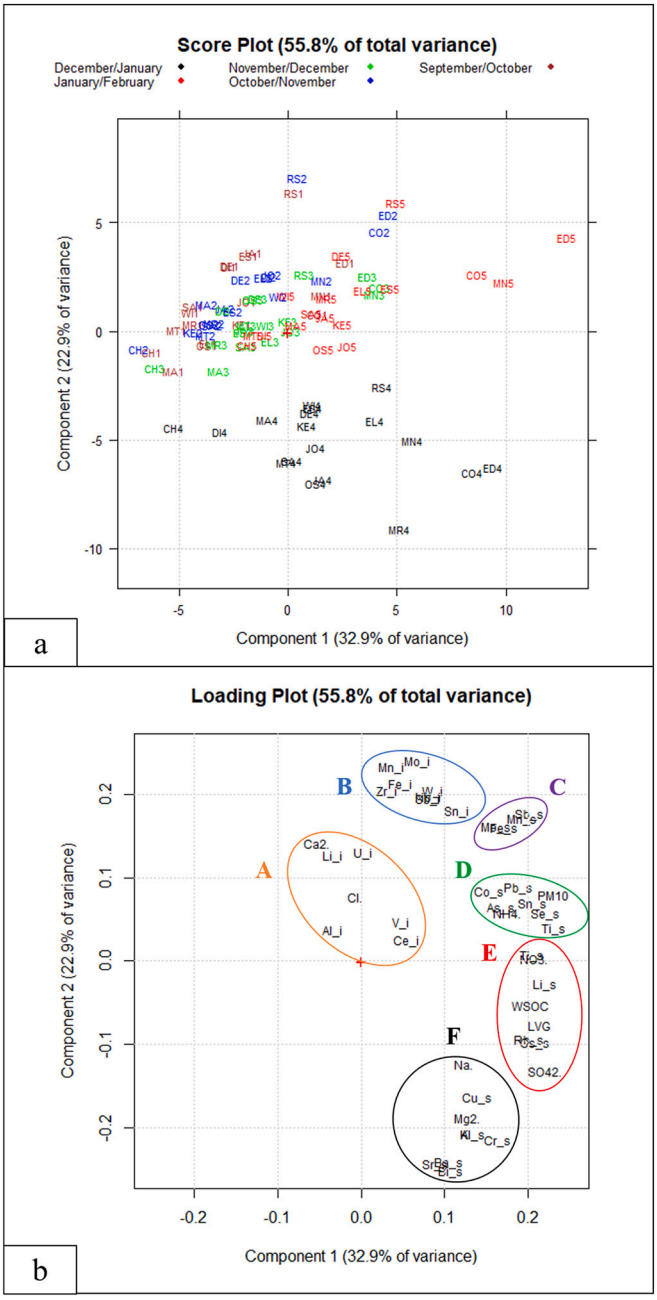

Fig. 3. Score (panel a) and loading (panel b) plot of the PCA (PC1/PC2) performed on the concentration data (ng m^{-3}) of PM_{10} mass and PM_{10} chemical compounds obtained at the 17 sampling sites in Amersfoort and at the regulatory reference site (RS) in Utrecht in the 5-month monitoring period.

sulfates and/or nitrates), whose production strongly depends on several chemical and micro-meteorological factors (Pathak et al., 2009) and can be enhanced by wood burning and fireworks episodes (Cheng et al., 2014). Therefore, in group E the chemical components that trace the secondary fraction of PM_{10} (both inorganic and organic) and PM_{10} particles released by biomass burning are clustered. Potassium ion is also usually deemed to be a reliable wood burning tracer, since it is produced by the combustion of biomass (Chow et al., 2007). However, it is plotted in group F instead of group E, because its concentration in PM_{10} was affected by the burning of New Year's Eve fireworks.

Second component (PC2) separates all the samples collected in the December/January monitoring period from the others, since they showed higher concentrations of K^+, Mg^{2+}, Na^+,Al_s, Ba_s, Bi_s, Cr_s, Cu_s and Sr_s (clustered in the group F), which are tracers of the burning of fireworks (Wang et al., 2007; Moreno et al., 2010; Tanda et al., 2019). As a confirmation of this, all these chemical compounds, in the December/January period, showed RSD > 50% (supplementary material S1) at site JO, where one of the two samplers used was stopped from 30/12/2018 to 3/1/2019 to assess the release of PM_{10} components due to the New Year's Eve fireworks. From Fig. 4, we can observe the different contribution in concentration of these compounds at JO due to the burning of fireworks during the five days in which one of the two samplers was stopped. These chemical components are contained in salts used to give white (K^+, Mg^{2+} and Al_s), silver (Mg^{2+}, Al_s, Cu_s and Cr_s), yellow (Na^+), green (Ba_s), blue (Cu_s) and red (Sr_s) colors to the fireworks; K^+, Cu_s and Cr_s are used to provide glitter effects, K^+ is also used as rocket propellant, while Mg^{2+}, Al_s and Bi_s are useful common metallic fuels to produce sparks, glitter and crackling stars (Russell, 2009; Nakatsubo et al., 2014; Tian et al., 2014).

It is worth noting that chromium is present on the vast majority of the water-soluble species as Cr(VI) (Brown et al., 2014), which has been classified as 'Group A carcinogen' by the U.S. Environmental Protection Agency (EPA; U.S. Environmental Protection Agency, 1984). Therefore, water-soluble Cr released by the burning of fireworks might be toxic. Moreover, PC2 clusters the samples collected at sites DE, ED and RS, containing higher concentrations of Fe_i, Mn_i, Mo_i, Nb_i, Sb_i, Sn_i, W_i and Zr_i (clustered in the group B), which were very likely released from non-exhaust vehicular traffic sources by abrasion and resuspension of vehicle/train brake disks and pads lining (Abbasi et al., 2012; Querol et al., 2012; Kam et al., 2013; Namgung et al., 2016; Massimi et al., 2020b). In fact, RS is a traffic regulatory reference site in Utrecht, while DE and ED are sites very close to the Amersfoort highways A1 and A28, respectively (Fig. 1; Table 2).

3.3. Spatial mapping of PM_{10} source tracers

The spatial distribution of the identified PM_{10} source tracers was mapped to delineate and localize the impact of the different emission sources acting in Amersfoort. Maps of the autumn and winter spatial distribution of PM_{10} mass concentration and of one representative tracer for each identified PM_{10} source (panel b; Fig. 3) are shown below.

From Fig. 5, we can observe that PM_{10} mass concentration increased at all the sampling sites in winter (panel b), due to more frequent episodes of atmospheric stability (Hendriks et al., 2013) and to the greater use of biomass domestic heating during the colder period, as previously discussed. Moreover, the transport of PM_{10} particles across the study area seems to have been driven by the predominant wind coming from the south (Gelaro et al., 2017), since the highest PM_{10} mass concentrations were recorded at ED, CO, EL and MN (Table 5), which are located along the south-north direction, in proximity of the two highways and of townhouses heated by biomass burning appliances (Fig. 1; Table 2), while the lowest concentrations were recorded at OS, MT, CH and MA (Table 4).

The elements analyzed in both the water-soluble and insoluble fraction (Al, Fe, Li, Mn, Mo, Sb and Sn) showed very different spatial distributions. As an example, the spatial maps of water-soluble and insoluble Li and Sn are reported in Fig. 6 (panels a-d) and Fig. 7 (panels a-d), respectively.

From Fig. 6, it can be seen that Li_s concentrations were clearly higher during the winter period (panel b) in the area where residential biomass combustion occurred (Fig. 1). The highest values were recorded, here too, at ED, CO, EL and MN (Table 5). The spatial distribution of Li_s (panels a, b) was almost identical to those of all the identified tracers of biomass burning (WSOC, LVG, Cs_s, Li_s, Rb_s and Tl_s) and secondary inorganic ions (NO_3^-, SO_4^{2-}), thus confirming the prevailing transport of the particles released from south to north. Spatial maps of all the analyzed chemical compounds are reported in supplementary material S4. On the contrary, the insoluble fraction of Li (panels c, d), a soil resuspension tracer (Canepari et al., 2008; Pant and Harrison, 2013;

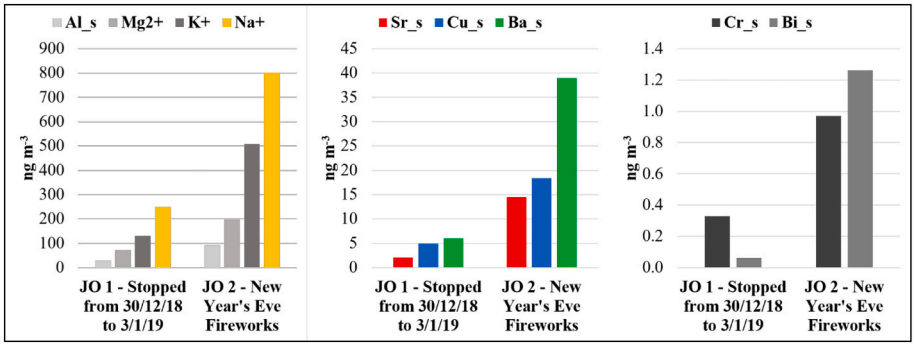

Fig. 4. Concentrations of K^+, Mg^{2+}, Na^+,Al_s, Ba_s, Bi_s, Cr_s, Cu_s and Sr_s released by the burning of New Year's Eve fireworks at JO.

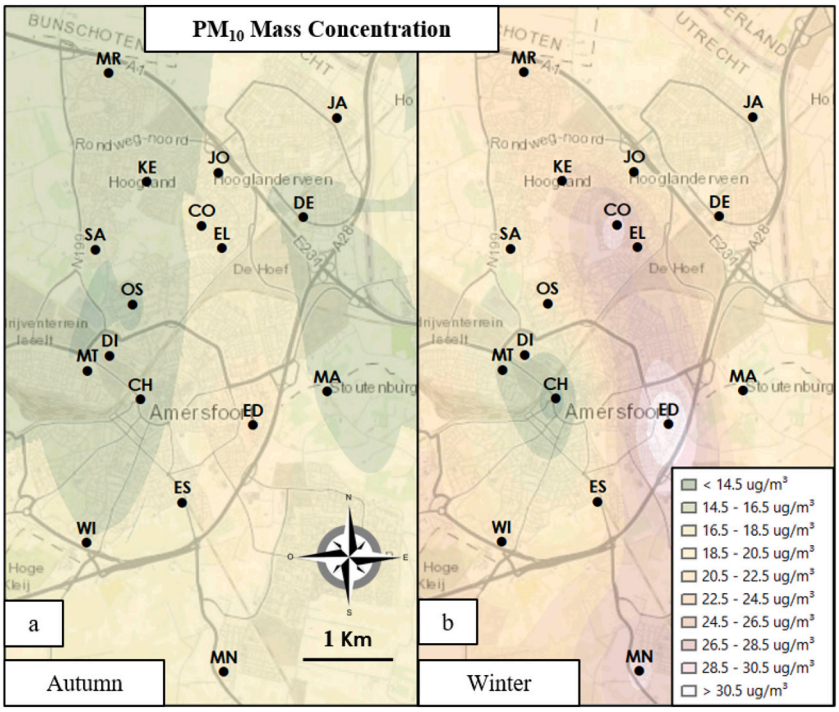

Fig. 5. Map of the autumn (panel a) and winter (panel b) spatial distribution of PM_{10} mass concentration.

Massimi et al., 2020b), showed a completely different seasonal variability and spatial distribution. In fact, its concentration was higher in autumn. Low spatial variability was observed for Li_i concentrations, revealing an homogeneous distribution of the soil dust, due to the lack of intensive soil local sources. A very similar behavior was observed also for all the other crustal components of PM_{10} (Ca^+, Cl^-, Al_i, Ce_i, Li_i, U_i and V_i).

From Fig. 7, we can observe that the concentrations of Sn_s, a tracer of industrial emissions (Fernández-Camacho et al., 2012; Canepari et al., 2014), were higher at KE, JO, ED, CO, EL, ES and MN, especially in winter (panel b) due to the stronger atmospheric stability. A practically identical spatial distribution was noted for all the other identified tracers of industrial and/or agricultural sources (NH_4^+, As_s, Co_s, Pb_s, Se_s, Sn_s and Ti_s). Peak concentrations were found at ES and MN (Table 5), which are sites in the southernmost area; it is thus conceivable that industrial and/or agricultural sources located further south or at the southern end of Amersfoort released particles that were transported to the study area by the predominant south wind. On the other hand, in autumn (panel c) as well as in winter (panel d), insoluble Sn concentrations were found to be higher at sites in proximity of trafficked streets, traffic lights, roundabouts, railway tracks, train stations and the highways A1 and A28 (Table 2), confirming vehicle/train brake abrasion as the main emission source of Sn_i. Indeed, the highest Sn_i concentrations were recorded in autumn at JO, DE, ED and ES (Table 4) and in winter at CO, EL, DE and ED (Table 5), which are all traffic sites. Concentrations of Sn_i did not considerably increased in winter, since brake abrasion is a mechanical process less sensitive to seasonal variations of atmospheric conditions (Canepari et al., 2019). A very similar spatial pattern was observed also for all the other brake dust tracers (Fe_i, Mn_i, Mo_i, Nb_i, Sb_i, W_i and Zr_i). Figs. 5 and 6 also show that water-soluble and insoluble species of Li and Sn were released into the atmosphere by different sources. This confirms the effectiveness of the chemical fractionation procedure in increasing the selectivity of the elements as source tracers (Perrino et al., 2010; Massimi et al., 2020b).

Finally, in Fig. 8, autumn and winter spatial maps of water-soluble Sb (panels a,b) and Bi (panels c,d) are reported. Water-soluble Sb, as well as Fe_s, Mn_s and Mo_s, showed a similar spatial distribution to that of the brake dust tracers in autumn (panel a) and to that of the tracers of industrial and/or agricultural emissions in winter (panel b). This because Sb_s was probably released by both industrial (Kim and Jo, 2006; Mbengue et al., 2014) and non-exhaust vehicular traffic emissions (Garg et al., 2000; Thorpe and Harrison, 2008).

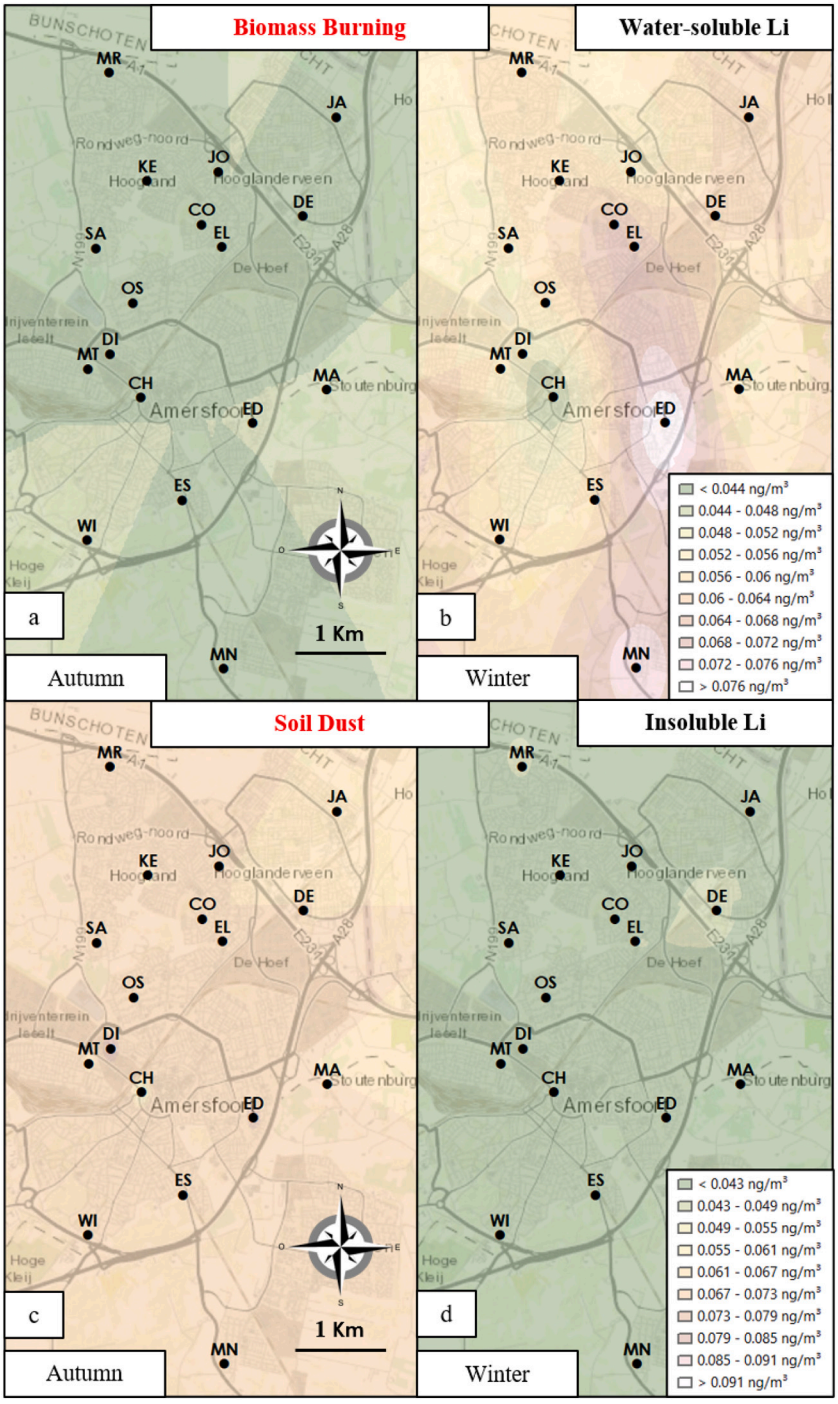

Fig. 6. Map of the autumn and winter spatial distribution of water-soluble Li (panels a,b) and insoluble Li (panels c,d).

Water-soluble Bi concentrations were found to be very low in autumn (panel c) and remarkably higher in winter (panel c) at all the sampling sites, since it was released by the burning of fireworks during the New Year's Eve, in the December/January monitoring period. In fact, as previously discussed, Bi_s is used in fireworks as metallic fuel to produce sparks, glitter and crackling stars. Its homogeneous spatial distribution reveals the widespread use of fireworks across the study area. The same behavior was observed also for all the other elements released by the burning of fireworks (K^+, Mg^{2+}, Na^+,Al_s, Ba_s, Cr_s, Cu_s and Sr_s).

4. Conclusions

The study of the autumn and winter spatial distribution of PM_{10} mass and PM_{10} chemical components in Amersfoort allowed us to identify, through the spatial mapping of chemical tracers of PM emissions, the main PM_{10} sources acting in the study area, and to evaluate the diffusion of the PM_{10} particles.

By applying the principal component analysis on the obtained spatially-resolved data, samples collected in each monitoring period at the different sites were clustered depending on the concentration variability of the PM_{10} chemical compounds. Selective and reliable source tracers were identified for soil dust (Ca^+, Cl^-, Al_i, Ce_i, Li_i, U_i and V_i),

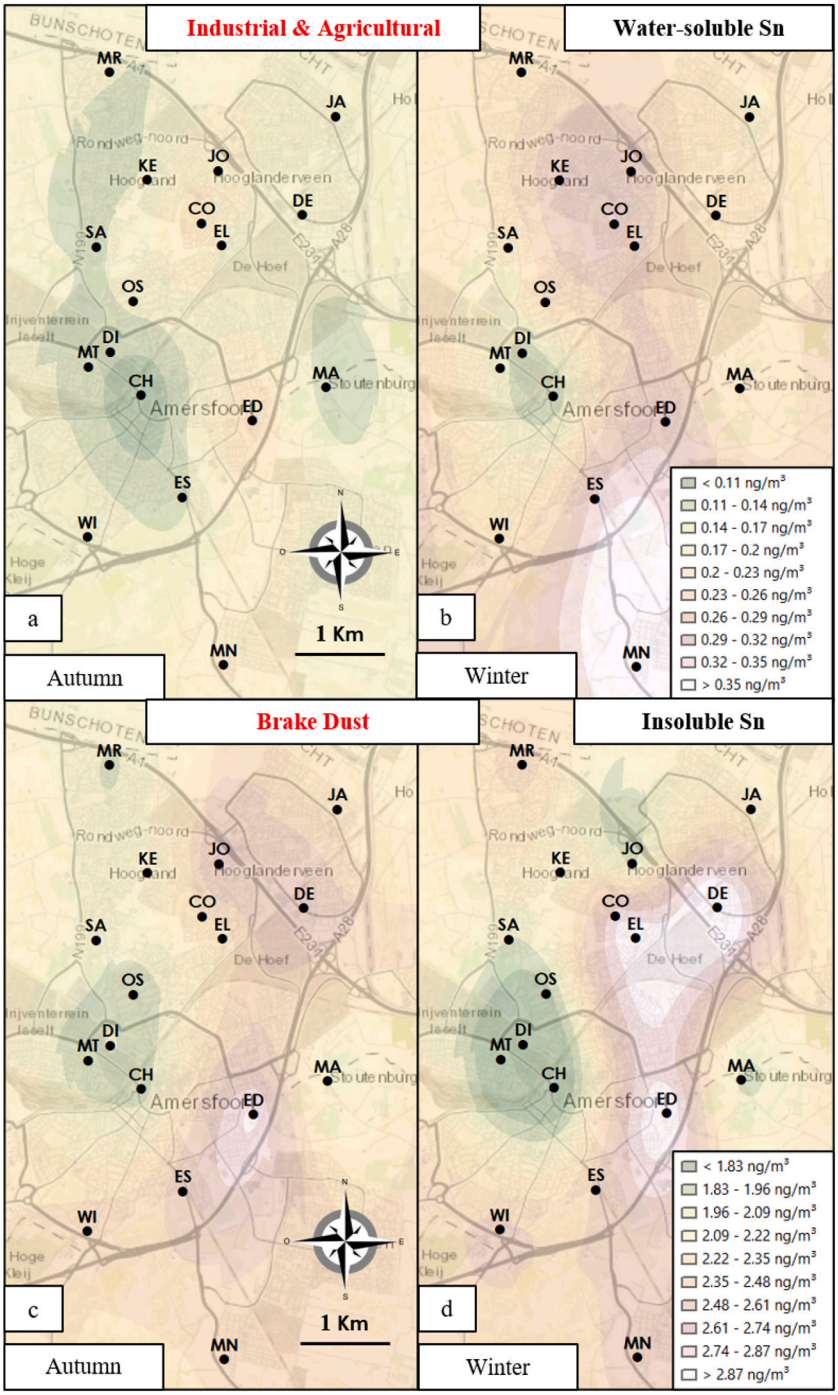

Fig. 7. Map of the autumn and winter spatial distribution of water-soluble Sn (panels a,b) and insoluble Sn (panels c,d).

brake dust (Fe_i, Fe_s, Mn_i, Mn_s, Mo_i, Mo_s Nb_i, Sb_i, Sb_s, Sn_i, W_i and Zr_i), industrial and/or agricultural emissions (NH_4^+, As_s, Co_s, Fe_s, Mn_s, Mo_s, Pb_s, Sb_s, Se_s, Sn_s and Ti_s), secondary organic and inorganic aerosols (WSOC, NO_3^- and SO_4^{2-}), biomass domestic heating (WSOC, LVG, Cs_s, Li_s, Rb_s and Tl_s) and the burning of New Year's Eve fireworks (K^+, Mg^{2+}, Na^+,Al_s, Ba_s, Bi_s, Cr_s, Cu_s and Sr_s).

A marked increase in PM_{10} mass concentration occurred at all the sites in winter, due to the stronger atmospheric stability and to the greater use of biomass domestic heating during the colder period. The transport of PM_{10} particles across the study area seems to have been driven by the predominant wind coming from the south.

Each identified source showed characteristic autumn and winter spatial distributions, depending on the sources strength and on the seasonal variation of atmospheric conditions. Soil dust emissions were found to be higher in autumn and widespread across the study area, brake dust appeared to be emitted in higher concentrations at the traffic sites in autumn as well as in winter, as expected. On the contrary, the chemical compounds contained in PM_{10} particles released by industrial and/or agricultural emissions were found to be more concentrated at the southern end of Amersfoort, especially in winter. A similar behavior was observed for the secondary organic and inorganic aerosols and for the biomass burning particles, which were found in higher concentration in winter, in the southern area, where biomass domestic heating systems were employed, especially in the colder period. Finally, PM_{10} particles released in winter by the burning of New Year's Eve fireworks showed a homogeneous distribution across the study area.

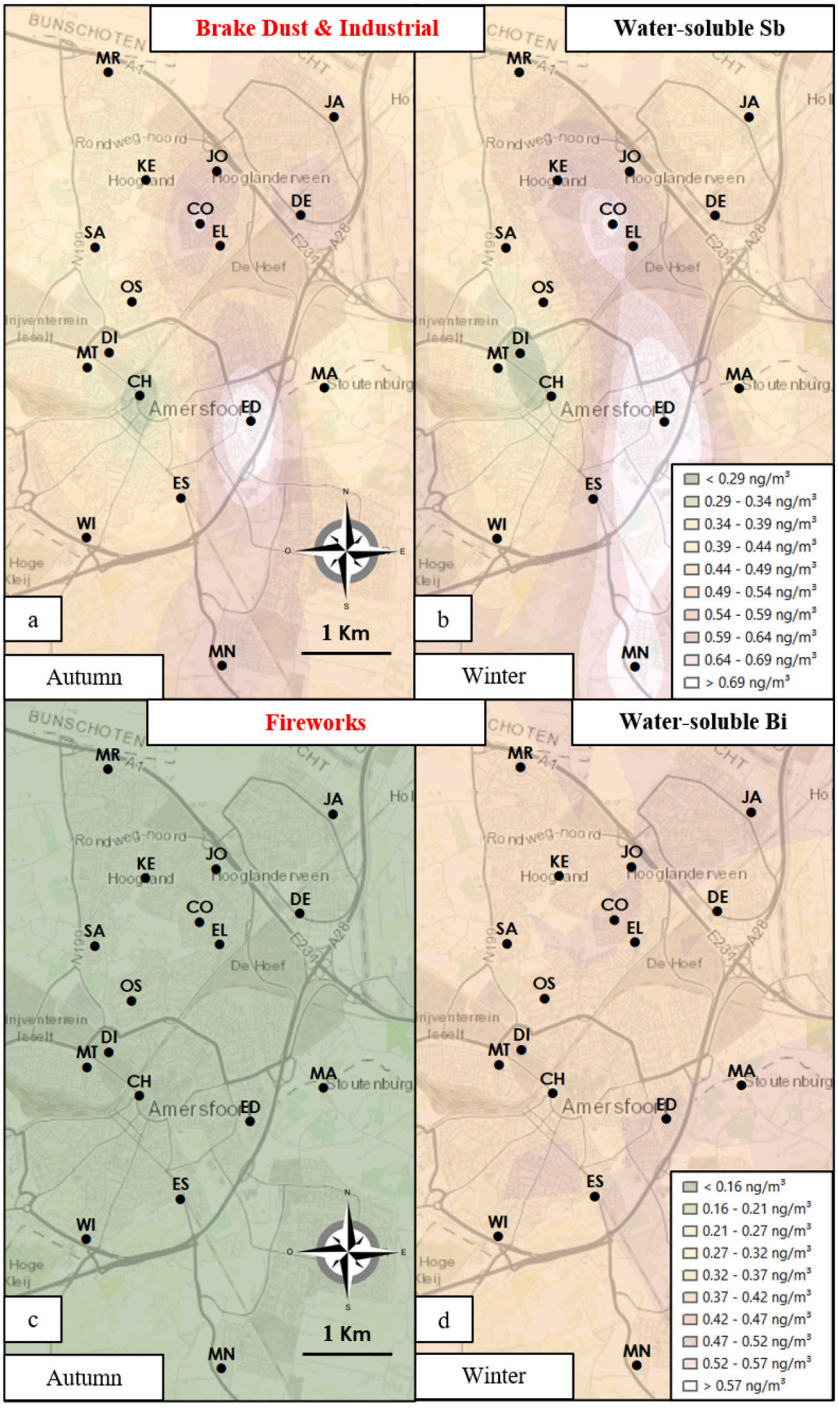

Fig. 8. Map of the autumn and winter spatial distribution of water-soluble Sb (panels a,b) and water-soluble Bi (panels c,d).

This experimental approach proved to be very effective to trace PM_{10} sources and to map their seasonal and spatial distribution in areas with weak emissions of PM, such as Amersfoort. Furthermore, it allowed us to overcome the limits connected to the study of PM diffusion through the use of mathematical models and the limits associated to the high cost of a traditional air quality monitoring network. Moreover, the acquired geo-referenced and spatially-resolved chemical data can be used in further studies to evaluate spatial relationships between the concentration of PM_{10} air pollutants and adverse outcomes for human health. Further investigations are necessary to achieve a full impact assessment of the PM_{10} sources in the study area and to plan the mitigation measures that are needed to protect citizens health.

This approach promises to be a powerful tool for obtaining seasonal and spatially-resolved information about PM composition and sources in several study areas that can be integrated with data from existing monitoring networks for a more reliable geo-referenced assessment of population exposure to PM, having high impact on the air quality management.

Author contributions

L. Massimi conceived and planned the monitoring and the experiments; L. Massimi, J. Wesseling and S. van Ratingen performed the samplings; L. Massimi, I. Javed, M.A. Frezzini and M. L. Astolfi

performed the chemical analyses; L. Massimi elaborated the data and wrote the manuscript; L. Massimi, S. Canepari and R. Vermeulen coordinated the group and supervised the manuscript.

Declaration of Competing Interest

The authors declare that they have no known competing financial interests or personal relationships that could have appeared to influence the work reported in this paper.

Acknowledgments

This work was funded by the projects 2018 AR1181641E22B570 and 2019 AR11916B7027C1E6 (Principal Investigator Dr. L. Massimi) financed by Sapienza University of Rome.

The authors thank FAI Instruments (Fonte Nuova, Rome, Italy), the citizens of Amersfoort, the Amersfoort city hall and the National Institute for Public Health and the Environment (RIVM, Bilthoven, Netherlands) for the support in the installation and management of the sampling equipment as well as for the help in the choice of the sampling sites. Moreover, the authors gratefully thank Cinzia Perrino and Elena Rantica of C.N.R. Institute of Atmospheric Pollution Research for performing part of the chemical analyses.

Appendix A. Supplementary data

Supplementary data to this article can be found online at https://doi.org/10.1016/j.atmosres.2021.105771.

References

Abbasi, S., Olander, L., Larsson, C., Olofsson, U., Jansson, A., Sellgren, U., 2012. A field test study of airborne wear particles from a running regional train. Proc. Inst. Mech. Eng. Part F: J. Rail Rapid Transit. 226 (1), 95–109.

Adler, G., Flores, J.M., Riziq, A.A., Borrmann, S., Rudich, Y., 2011. Chemical, physical, and optical evolution of biomass burning aerosols: a case study. Atmos. Chem. Phys. 11 (4), 1491.

Astolfi, M.L., Canepari, S., Catrambone, M., Perrino, C., Pietrodangelo, A., 2006. Improved characterisation of inorganic components in airborne particulate matter. Environ. Chem. Lett. 3, 186–191.

Astolfi, M.L., Di Filippo, P., Gentili, A., Canepari, S., 2017. Semiautomatic sequential extraction of polycyclic aromatic hydrocarbons and elemental bio-accessible fraction by accelerated solvent extraction on a single particulate matter sample. Talanta 174, 838–844.

Astolfi, M.L., Protano, C., Marconi, E., Massimi, L., Brunori, M., Piamonti, D., Migliara, G., Vitali, M., Canepari, S., 2020. A new treatment of human hair for elemental determination by inductively coupled mass spectrometry. Anal. Methods 12, 1906–1918.

Battye, W., Aneja, V.P., Roelle, P.A., 2003. Evaluation and improvement of ammonia emissions inventories. Atmos. Environ. 37 (27), 3873–3883.

Belis, C.A., Karagulian, F., Amato, F., Almeida, M., Artaxo, P., Beddows, D.C.S., Hopke, P. K., 2015. A new methodology to assess the performance and uncertainty of source apportionment models II: the results of two European intercomparison exercises. Atmos. Environ. 123, 240–250.

Brown, R.J., Van Aswegen, S., Webb, W.R., Goddard, S.L., 2014. UK concentrations of chromium and chromium (VI), measured as water soluble chromium, in PM10. Atmos. Environ. 99, 385–391.

Canepari, S., Cardarelli, Giuliano A.E., Pietrodangelo, A., 2006a. Determination of metals, metalloids and non-volatile ions in airborne particulate matter by a new two-step sequential leaching procedure part A: Experimental design and optimization. Talanta 69 (3), 581–587.

Canepari, S., Cardarelli, E., Pietrodangelo, A., Strincone, M., 2006b. Determination of metals, metalloids and non-volatile ions in airborne particulate matter by a new two-step sequential leaching procedure: Part B: Validation on equivalent real samples. Talanta 69 (3), 588–595.

Canepari, S., Perrino, C., Olivieri, F., Astolfi, M.L., 2008. Characterisation of the traffic sources of PM through size-segregated sampling, sequential leaching and ICP analysis. Atmos. Environ. 42 (35), 8161–8175.

Canepari, S., Pietrodangelo, A., Perrino, C., Astolfi, M.L., Marzo, M.L., 2009. Enhancement of source traceability of atmospheric PM by elemental chemical fractionation. Atmos. Environ. 43 (31), 4754–4765.

Canepari, S., Astolfi, M.L., Farao, C., Maretto, M., Frasca, D., Marcoccia, M., Perrino, C., 2014. Seasonal variations in the chemical composition of particulate matter: a case study in the Po Valley. Part II: concentration and solubility of micro-and trace-elements. Environ. Sci. Pollut. Res. 21 (6), 4010–4022.

Canepari, S., Astolfi, M.L., Catrambone, M., Frasca, D., Marcoccia, M., Marcovecchio, F., Massimi, L., Rantica, E., Perrino, C., 2019. A combined chemical/size fractionation approach to study winter/summer variations, ageing and source strength of atmospheric particles. Environ. Pollut. 253, 19–28.

Catrambone, M., Canepari, S., Cerasa, M., Sargolini, T., Perrino, C., 2019. Performance evaluation of a very-low-volume sampler for atmospheric particulate matter. Aerosol Air Qual. Res. 19 (10), 2160–2172.

Chen, J., Hoek, G., 2020. Long-term exposure to PM and all-cause and cause-specific mortality: a systematic review and meta-analysis. Environ. Int. 105974.

Cheng, Y., Engling, G., He, K.B., Duan, F.K., Du, Z.Y., Ma, Y.L., Liang, L., Lu, Z., Liu, J., Zheng, M., Weber, R.J., 2014. The characteristics of Beijing aerosol during two distinct episodes: Impacts of biomass burning and fireworks. Environ. Pollut. 185, 149–157.

Chow, J.C., Watson, J.G., Lowenthal, D.H., Chen, L.W.A., Zielinska, B., Mazzoleni, L.R., Magliano, K.L., 2007. Evaluation of organic markers for chemical mass balance source apportionment at the Fresno Supersite. Atmosph. Chem. Phys. 7 (7), 1741–1754. https://doi.org/10.5194/acp-7-1741-2007.

Conti, M.E., Iacobucci, M., Cucina, D., Mecozzi, M., 2007. Multivariate statistical methods applied to biomonitoring studies. Int. J. Environ. Pollut. 29 (1–3), 333–343.

Engling, G., Herckes, P., Kreidenweis, S.M., Malm, W.C., Collett Jr., J.L., 2006. Composition of the fine organic aerosol in Yosemite National Park during the 2002 Yosemite Aerosol Characterization Study. Atmos. Environ. 40 (16), 2959–2972.

Ervens, B.T.B.W.R., Turpin, B.J., Weber, R.J., 2011. Secondary organic aerosol formation in cloud droplets and aqueous particles (aqSOA): a review of laboratory, field and model studies. Atmosph. Chem. Phys. Discus. 11 (8).

Fernández-Camacho, R., Rodríguez, S., De la Rosa, J., de la Campa, A.S., Alastuey, A., Querol, X., González-Castanedo, Y., Garcia-Orellana, I., Nava, S., 2012. Ultrafine particle and fine trace metal (As, Cd, Cu, Pb and Zn) pollution episodes induced by industrial emissions in Huelva, SW Spain. Atmos. Environ. 61, 507–517.

Fischer, P.H., Marra, M., Ameling, C.B., Velders, G.J., Hoogerbrugge, R., de Vries, W., Wesseling, J., Janssen, N.A.H., Houthuijs, D., 2020. Particulate air pollution from different sources and mortality in 7.5 million adults - the Dutch Environmental Longitudinal Study (DUELS). Sci. Total Environ. 705, 135778.

Frasca, D., Marcoccia, M., Tofful, L., Simonetti, G., Perrino, C., Canepari, S., 2018. Influence of advanced wood-fired appliances for residential heating on indoor air quality. Chemosphere 211, 62–71.

Garg, B.D., Cadle, S.H., Mulawa, P.A., Groblicki, P.J., Laroo, C., Parr, G.A., 2000. Brake wear particulate matter emissions. Environ. Sci. Technol. 34 (21), 4463–4469.

Gelaro, R., McCarty, W., Suárez, M.J., Todling, R., Molod, A., Takacs, L., Randles, C.A., Darmenov, A., Bosilovich, M.G., Reichle, R., Wargan, K., Coy, L., Cullather, R., Draper, C., Akella, S., Buchard, V., Conaty, A., da Silva, A.M., Gu, W., Kim, G., Koster, R., Lucchesi, R., Merkova, D., Nielsen, J.E., Partyka, G., Pawson, S., Putman, W., Rienecker, M., Schubert, S.D., Sienkiewicz, M., Zhao, B., 2017. The modern-era retrospective analysis for research and applications, version 2 (MERRA-2). J. Clim. 30 (14), 5419–5454.

Graham, B., Mayol-Bracero, O.L., Guyon, P., Roberts, G.C., Decesari, S., Facchini, M.C., Fuzzi, S., Andreae, M.O., 2002. Water-soluble organic compounds in biomass burning aerosols over Amazonia 1. Characterization by NMR and GC-MS. J. Geophys. Res.-Atmos. 107 (D20), LBA–14.

Greven, F.E., Vonk, J.M., Fischer, P., Duijm, F., Vink, N.M., Brunekreef, B., 2019. Air pollution during New Year's fireworks and daily mortality in the Netherlands. Sci. Rep. 9 (1), 1–8.

Hendriks, C., Kranenburg, R., Kuenen, J., van Gijlswijk, R., Kruit, R.W., Segers, A., van der Gon, H.D., Schaap, M., 2013. The origin of ambient particulate matter concentrations in the Netherlands. Atmos. Environ. 69, 289–303.

Jian, X., Olea, R.A., Yu, Y.S., 1996. Semivariogram modeling by weighted least squares. Comput. Geosci. 22 (4), 387–397.

Johnston, K., Ver Hoef, J.M., Krivoruchko, K., Lucas, N., 2001. Using ArcGIS Geostatistical Analyst, 380 (Esri).

Kam, W., Delfino, R.J., Schauer, J.J., Sioutas, C., 2013. A comparative assessment of $PM_{2.5}$ exposures in light-rail, subway, freeway, and surface street environments in Los Angeles and estimated lung cancer risk. Environ Sci Process Impacts 15 (1), 234–243.

Kim, M.K., Jo, W.K., 2006. Elemental composition and source characterization of airborne PM 10 at residences with relative proximities to metal-industrial complex. Int. Arch. Occup. Environ. Health 80 (1), 40–50.

Kloog, I., Ridgway, B., Koutrakis, P., Coull, B.A., Schwartz, J.D., 2013. Long- and short term exposure to $PM_{2.5}$ and mortality using novel exposure models. Epidemiology 24, 555–561.

Knaapen, A.M., Shi, T., Borm, P.J., Schins, R.P., 2002. Soluble metals as well as the insoluble particle fraction are involved in cellular DNA damage induced by particulate matter. In: Oxygen/Nitrogen Radicals: Cell Injury and Disease. Springer, Boston, MA, pp. 317–326.

Korhonen, A., Lehtomäki, H., Rumrich, I., Karvosenoja, N., Paunu, V.V., Kupiainen, K., Sofiev, M., Palamarchuk, Y., Kukkonen, L., Kangas, L., Karppinen, A., Hänninen, O., 2019. Influence of spatial resolution on population PM 2.5 exposure and health impacts. Air Qual. Atmos. Health 12 (6), 705–718.

Kumar, A., Maroju, S., Bhat, A., 2007. Application of ArcGIS geostatistical analyst for interpolating environmental data from observations. Environ. Prog. 26 (3), 220–225.

Leardi, R., Melzi, C., Polotti, G.. CAT (Chemometric Agile Tool). Available online. http://gruppochemiometria.it/index.php/software (accessed on 1 February 2020).

Lee, S., Kim, H.K., Yan, B., Cobb, C.E., Hennigan, C., Nichols, S., Chamber, M., Edgerton, E.S., Jansen, J.J., Hu, Y.T., Zheng, M., Weber, R.J., Russell, A.G., 2008. Diagnosis of aged prescribed burning plumes impacting an urban area. Environ. Sci. Technol. 42 (5), 1438–1444.

Massimi, L., Ristorini, M., Eusebio, M., Florendo, D., Adeyemo, A., Brugnoli, D., Canepari, S., 2017. Monitoring and evaluation of Terni (Central Italy) air quality through spatially resolved analyses. Atmosphere 8 (10), 200.

Massimi, L., Simonetti, G., Buiarelli, F., Di Filippo, P., Pomata, D., Riccardi, C., Ristorini, M., Astolfi, M.L., Canepari, S., 2020a. Spatial distribution of levoglucosan and alternative biomass burning tracers in atmospheric aerosols, in an urban and industrial hot-spot of Central Italy. Atmos. Res. 104904.
Massimi, L., Ristorini, M., Astolfi, M.L., Perrino, C., Canepari, S., 2020b. High resolution spatial mapping of element concentrations in PM10: A powerful tool for localization of emission sources. Atmos. Res. 105060.
Mbengue, S., Alleman, L.Y., Flament, P., 2014. Size-distributed metallic elements in submicronic and ultrafine atmospheric particles from urban and industrial areas in northern France. Atmos. Res. 135, 35–47.
Minguillón, M.C., Cirach, M., Hoek, G., Brunekreef, B., Tsai, M., de Hoogh, K., Jedynskag, A., Kooterg, I.M., Nieuwenhuijsen, M., Querol, X., 2014. Spatial variability of trace elements and sources for improved exposure assessment in Barcelona. Atmos. Environ. 89, 268–281.
Mooibroek, D., Schaap, M., Weijers, E.P., Hoogerbrugge, R., 2011. Source apportionment and spatial variability of PM2. 5 using measurements at five sites in the Netherlands. Atmos. Environ. 45 (25), 4180–4191.
Moreno, T., Querol, X., Alastuey, A., Amato, F., Pey, J., Pandolfi, M., Kuenzli, N., Bouso, L., Rivera, M., Gibbons, W., 2010. Effect of fireworks events on urban background trace metal aerosol concentrations: is the cocktail worth the show? J. Hazard. Mater. 183 (1–3), 945–949.
Nakatsubo, R., Tsunetomo, D., Horie, Y., Hiraki, T., Saitoh, K., Yoda, Y., Shima, M., 2014. Estimate of regional and broad-based sources for PM 2.5 Collected in an Industrial Area of Japan. Asian J. Atmosph. Environ. (AJAE) 8 (3).
Namgung, H.G., Kim, J.B., Woo, S.H., Park, S., Kim, M., Kim, M.S., Bae, G.N., Park, D., Kwon, S.B., 2016. Generation of nanoparticles from friction between railway brake disks and pads. Environ. Sci. Technol. 50 (7), 3453–3461.
Øvrevik, J., 2019. Oxidative potential versus biological effects: a review on the relevance of cell-free/abiotic assays as predictors of toxicity from airborne particulate matter. Int. J. Mol. Sci. 20, 4772.
Pant, P., Harrison, R.M., 2013. Estimation of the contribution of road traffic emissions to particulate matter concentrations from field measurements: a review. Atmos. Environ. 77, 78–97.
Paramasivam, C.R., Venkatramanan, S., 2019. An introduction to various spatial analysis techniques. GIS Geostatist. Techn. Groundwater Sci. 3, 23–30.
Park, S.S., Cho, S.Y., Jo, M.R., Gong, B.J., Park, J.S., Lee, S.J., 2014. Field evaluation of a near–real time elemental monitor and identification of element sources observed at an air monitoring supersite in Korea. Atmosph. Poll. Res. 5 (1), 119–128.
Pathak, R.K., Wu, W.S., Wang, T., 2009. Summertime PM 2.5 ionic species in four major cities of China: nitrate formation in an ammonia-deficient atmosphere. Atmosph. Chem. Phys. 9 (5), 1711–1722.
Perrino, C., Canepari, S., Pappalardo, S., Marconi, E., 2010. Time-resolved measurements of water-soluble ions and elements in atmospheric particulate matter for the characterization of local and long-range transport events. Chemosphere 80 (11), 1291–1300.
Perrino, C., Tofful, L., Dalla Torre, S., Sargolini, T., Canepari, S., 2019. Biomass burning contribution to PM10 concentration in Rome (Italy): Seasonal, daily and two-hourly variations. Chemosphere 222, 839–848.
Pope III, C.A., Dockery, D.W., 2006. Health effects of fine particulate air pollution: Lines that connect. J. Air Waste Manage. Assoc. 56, 709–742.
Pozzer, A., Tsimpidi, A.P., Karydis, V.A., De Meij, A., Lelieveld, J., 2017. Impact of agricultural emission reductions on fine-particulate matter and public health. Atmos. Chem. Phys. 17 (20), 12813.
Querol, X., Moreno, T., Karanasiou, A., Reche, C., Alastuey, A., Viana, M., Font, O., Gil, J., de Miguel, E., Capdevila, M., 2012. Variability of levels and composition of PM_{10} and $PM_{2.5}$ in the Barcelona metro system. Atmos. Chem. Phys. 12 (11), 5055–5076.
Russell, M.S., 2009. The Chemistry of Fireworks. Royal Society of Chemistry.
Saarikoski, S., Sillanpää, M., Sofiev, M., Timonen, H., Saarnio, K., Teinilä, K., Karppinen, A., Kukkonen, J., Hillamo, R., 2007. Chemical composition of aerosols during a major biomass burning episode over northern Europe in spring 2006: experimental and modelling assessments. Atmosph. Environ. 41 (17), 3577–3589.
Schauer, J.J., Kleeman, M.J., Cass, G.R., Simoneit, B.R., 2001. Measurement of emissions from air pollution sources. 3. C1− C29 organic compounds from fireplace combustion of wood. Environ. Sci. Technol. 35 (9), 1716–1728.
Schmitz, O., Beelen, R., Strak, M., Hoek, G., Soenario, I., Brunekreef, B., Vaartjes, I., Dijst, M.J., Grobbee, D.E., Karssenberg, D., 2019. High resolution annual average air pollution concentration maps for the Netherlands. Sci. Data 6, 190035.
Setton, E., Marshall, J.D., Brauer, M., Lundquist, K.R., Hystad, P., Keller, P., Cloutier Fisher, D., 2010. The impact of daily mobility on exposure to traffic-related air pollution and health effect estimates. J. Expos. Sci. Environ. Epidemiol. 21, 42–48.
Shen, J., Liu, X., Zhang, Y., Fangmeier, A., Goulding, K., Zhang, F., 2011. Atmospheric ammonia and particulate ammonium from agricultural sources in the North China Plain. Atmos. Environ. 45 (28), 5033–5041.
Simoneit, B.R., Schauer, J.J., Nolte, C.G., Oros, D.R., Elias, V.O., Fraser, M.P., Rogge, W. F., Cass, G.R., 1999. Levoglucosan, a tracer for cellulose in biomass burning and atmospheric particles. Atmos. Environ. 33 (2), 173–182.
Simoneit, B.R., Elias, V.O., Kobayashi, M., Kawamura, K., Rushdi, A.I., Medeiros, P.M., Rogge, W.F., Didyk, B.M., 2004. Sugars dominant water-soluble organic compounds in soils and characterization as tracers in atmospheric particulate matter. Environ. Sci. Technol. 38 (22), 5939–5949.
Simonetti, G., Frasca, D., Marcoccia, M., Farao, C., Canepari, S., 2018. Multi-elemental analysis of particulate matter samples collected by a particle-into-liquid sampler. Atmosph. Poll. Res. 9 (4), 747–754.
Strak, M., Janssen, N.A., Godri, K.J., Gosens, I., Mudway, I.S., Cassee, F.R., Lebret, E., Kelly, F.G., Harrison, M.R., Brunekreef, B., Steenhof, M., Hoek, G., 2012. Respiratory health effects of airborne particulate matter: the role of particle size, composition, and oxidative potential - the RAPTES project. Environ. Health Perspect. 120 (8), 1183–1189.
Sullivan, A.P., Holden, A.S., Patterson, L.A., McMeeking, G.R., Kreidenweis, S.M., Malm, W.C., Hao, W.M., Wold, C.E., Collett Jr., J.L., 2008. A method for smoke marker measurements and its potential application for determining the contribution of biomass burning from wildfires and prescribed fires to ambient PM2.5 organic carbon. J. Geophys. Res.-Atmos. 113 (D22).
Tanda, S., Ličbinský, R., Hegrová, J., Goessler, W., 2019. Impact of New Year's Eve fireworks on the size resolved element distributions in airborne particles. Environ. Int. 128, 371–378.
Thorpe, A., Harrison, R.M., 2008. Sources and properties of non-exhaust particulate matter from road traffic: a review. Sci. Total Environ. 400 (1–3), 270–282.
Tian, Y.Z., Wang, J., Peng, X., Shi, G.L., Feng, Y.C., 2014. Estimation of the direct and indirect impacts of fireworks on the physicochemical characteristics of atmospheric PM10 and PM2. 5. Atmos. Chem. Phys. 9469.
Toro, R., Downward, G.S., van der Mark, M., Brouwer, M., Huss, A., Peters, S., Hoek, G., Nijssen, P., Wim, M., Sas, A., Laar, T., Kromhout, H., Vermeulen, R., 2019. Parkinson's disease and long-term exposure to outdoor air pollution: a matched case-control study in the Netherlands. Environ. Int. 129, 28–34.
U.S. Environmental Protection Agency, 1984. U.S. Environmental Protection Agency. Health Effects Assessment for Hexavalent Chromium, EPA 540/1–86-019. U.S. EPA, Washington DC (1984).
Urban, R.C., Lima-Souza, M., Caetano-Silva, L., Queiroz, M.E.C., Nogueira, R.F., Allen, A. G., Cardoso, A.A., Held, G., Campos, M.L.A., 2012. Use of levoglucosan, potassium, and water-soluble organic carbon to characterize the origins of biomass-burning aerosols. Atmos. Environ. 61, 562–569.
Wang, Y., Zhuang, G., Xu, C., An, Z., 2007. The air pollution caused by the burning of fireworks during the lantern festival in Beijing. Atmos. Environ. 41 (2), 417–431.
Weber, R.J., Sullivan, A.P., Peltier, R.E., Russell, A., Yan, B., Zheng, M., de Gouw, J., Warneke, C., Brock, C., Holloway, J.S., Atlas, E.L., Edgerton, E., 2007. A study of secondary organic aerosol formation in the anthropogenic-influenced southeastern United States. J. Geophys. Res.-Atmos. 112 (D13).
Xie, Y., Chen, T.B., Lei, M., Yang, J., Guo, Q.J., Song, B., Zhou, X.Y., 2011. Spatial distribution of soil heavy metal pollution estimated by different interpolation methods: Accuracy and uncertainty analysis. Chemosphere 82 (3), 468–476.